

Melamine-crosslinked Polyimide Aerogels from Supercritical Ethanol Drying with Improved In-use Shape Stability Against Shrinking

Weiwan Chen ¹, Sha Liu ¹, Yueyan Sun ¹, Xiaomeng Zhou ^{1*}, Fenglei Zhou ^{2,3}

¹ Key Laboratory of Civil Aviation Thermal Hazards Prevention and Emergency Response, Civil Aviation University of China, Tianjin 300300, PR China

² Centre for Medical Image Computing, Department of Computer Science, University College London, London WC1V 6LJ, UK

³ College of Textiles and Clothing, Qingdao University, Qingdao 266071, PR China

Corresponding Author: X. Zhou (Email: zhouxm@nankai.edu.cn)

Abstract

Polyimide aerogels are promising for diverse applications owing to their nano-porous structure and superior properties. However, the shrinkage of melamine-crosslinked polyimide (MPI) aerogels has greatly compromised their performance in practical applications. In this study, supercritical drying with ethanol rather than CO₂ is employed to enhance their in-use shape stability at high temperatures. The structure, thermal insulation, mechanical strength of the resultant aerogels as well as their shape stability are characterized. Experimental results reveal that the shape stability of MPI aerogels during use is greatly improved thanks to the in-advance baptism of supercritical ethanol drying. The aerogel shrinks by only 2.64 vol.% after being treated at 280 °C for 72 h. Besides, the MPI aerogel shows enhanced compressive strength and can easily support a load more than 20, 000 times its own weight. The thermal conductivity of these aerogels varies from 0.034 W·m⁻¹·k⁻¹ to 0.046 W·m⁻¹·k⁻¹, indicative of remarkable performance in thermal insulation. In addition, the aerogels that started to decompose at as high as 500 °C also perform well in thermal stability and char forming. It can be envisaged that the developed MPI aerogels with greatly improved in-use shape stability may have broad prospects for thermal insulation at high temperatures.

Keywords

Polyimide Aerogels, Shrinkage, Supercritical Drying, Shape Stability, Thermal Insulation

1. Introduction

Due to their unique nano-porous nature, ultralight densities, low thermal conductivity, etc., polymer aerogels have received a lot of attention in the fields of thermal insulation, catalysis, waste disposal, and so on [1-4]. Up to now, there are a wide variety of polymer aerogels available, such as those derived from phenolic resins (PR) [5], polybenzoxazines (PBO) [6, 7], polyureas (PUA) [8], KevlarTM-like polyamides (PPTA) [9, 10], polyimides (PI) [11-13], polyurethanes (PU) [14], etc. Among them, PI aerogels are very attractive due to their superior mechanical and thermal insulation properties, and can find diverse applications such as extravehicular activity (EVA) suits, thermal protective systems (TPS), submarine sound barrier systems, etc. [15]

To obtain high-performance PI aerogels in a cost-effective way, a series of melamine-crosslinked polyimide (MPI) aerogels with melamine as an accessible and economical crosslinker were prepared in our previous study [16]. The resultant MPI aerogels dried by supercritical CO₂ were tested to have low shrinkage (as low as 9.96 vol.%), ultralight bulk densities (0.084-0.116 g·cm⁻³) and low thermal conductivity (< 0.04 W·m⁻¹·k⁻¹), as well as considerable thermal stability and acceptable compressive strength. However, these aerogels tend to suffer severe volume shrinkage when exposed to high temperatures, due to the removal of possible residual solvent, moisture and CO₂ adsorbed. This will bring great unreliability to the practical application of MPI aerogels. Further efforts therefore are still needed to improve the in-use shape stability of MPI aerogels against shrinking.

It has been reported that the shrinkage of PI aerogels can be reduced by adjusting the monomers, filling fibers, or changing the procedure of preparation [17-21]. M. A. B. Meador et al. (2015), for example, found that the PI aerogels derived from 4, 4'-oxydianiline (ODA) always shrink more than those derived from dimethylbenzidine

(DMBZ) [17]. That is, the shrinkage of PI aerogels can be regulated by adjusting the ratio of DMBZ to ODA. Z. Zhu et al. (2019) added glass fiber mat to PI aerogels in the process of aerogel preparation, to reduce the aerogel's shrinkage [18]. The introduction of fiber mat did result in less shrinkage values of 7.8-9.7 %. X. Zhang et al. (2020) used bacterial cellulose (BC) as the reinforcing nanofiller for PI aerogels [20]. The aerogel's linear shrinkage decreased from 36 % to 17 % when 40 wt.% of BC was incorporated, which indicates that the shrinkage of PI aerogels during preparation was significantly inhibited by adding BC into the matrix. However, these studies mainly focused on reducing the shrinkage of PI aerogels in the process of preparation, rather than in use. The in-use stability of these PI aerogels against shrinkage at high temperatures is still unclear, as a lower shrinkage for PI aerogels during preparation does not necessarily guarantee a better shape stability in use, just like what we learned from the MPI aerogels. Besides, in order to improve the shrinkage resistance of PI aerogels, additional heterogeneous supports such as fibers were often needed. This will inevitably degrade the thermal insulation performance of PI aerogels. Even so, there seem to be no other better choices. Neat PI aerogels that perform well in shape stability during use are worth pursuing.

In the present study, we proposed to use ethanol instead of CO₂ for supercritical drying to prepare neat MPI aerogels with high in-use stability against shrinkage, without adding any other supporting materials. This is to allow the aerogels to endure the high temperature of supercritical ethanol in advance, and therefore to avoid shrinkage when used at such high temperatures. The structure, thermal insulation, compressive strength of the modified MPI aerogels as well as their shape stability for high-temperature applications were characterized. The experimental results revealed that the in-use shape stability of MPI aerogels at high temperatures was greatly improved as expected, thanks

to the baptism of supercritical ethanol drying. Besides, MPI aerogels dried by supercritical ethanol also performed well in heat insulation, thermal endurance, and compression resistance. These advantages enable the MPI aerogels to be promising for high-temperature applications including thermal insulation.

2. Experimental

2.1 Materials

Dimethylbenzidine (DMBZ), 4, 4'-oxydianiline (ODA), 4, 4'-oxydiphthalic anhydride (ODPA), N-methylpyrrolidinone (NMP) and melamine were purchased from Shanghai Aladdin Biochemical Technology Co., Ltd (Shanghai, China). Propionic anhydride was supplied by Nanjing Chemical Reagent Co., Ltd (Nanjing, China). Pyridine was provided by Alfa-Aesar (China) Chemical Co., Ltd (Shanghai, China).

2.2 Preparation of MPI Aerogels

MPI aerogels were prepared by using hybrid diamines of DMBZ and ODA with melamine as an economical yet effective crosslinker, according to our previous work [16]. The synthetic route to melamine-crosslinked polyimide is given in **Figure S1** in the **Supplementary Material**. Somewhat different from our previous work, ethanol instead of CO₂ was used for supercritical drying, which allowed the aerogels to endure the supercritical high temperature of ethanol in advance and therefore gained the ability to resist shrinking during use. The procedure for preparing MPI aerogels is shown in **Figure 1**. For comparison, we use MPI-C-*x* and MPI-E-*x* to distinguish the obtained aerogels, where C and E represent the supercritical fluids for drying, i.e., CO₂ and ethanol, respectively. To in line with our previous study, the *x* here also denotes the weight percent of DMBZ in hybrid diamines (DMBZ content in short).

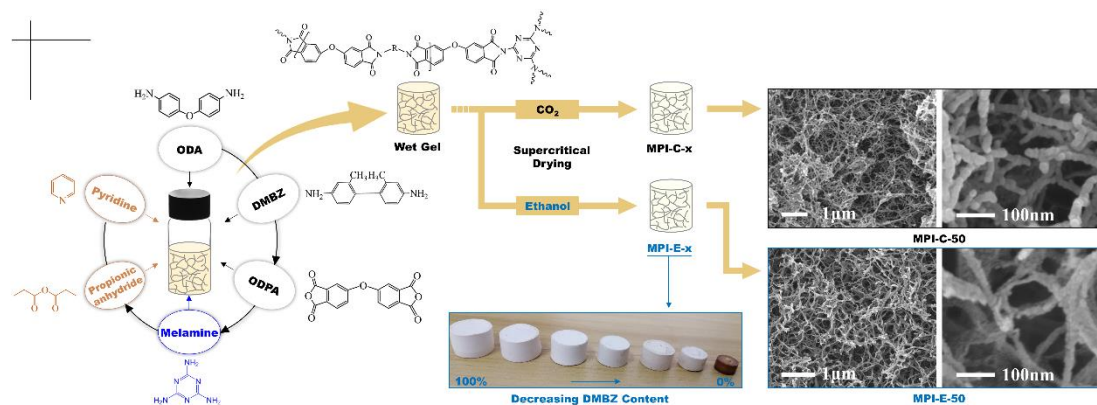


Figure 1. The procedure for preparing MPI aerogels from supercritical ethanol and CO₂ drying.

2.3 Characterization

The bulk density of MPI aerogels was calculated from the corresponding mass-to-volume ratios. The morphology of the prepared MPI aerogels was observed by field emission scanning electron microscopy (FE-SEM, LEO-1530VP, ZEISS, Germany). Prior to SEM observations, the samples were sputter-coated with gold to render them better electrical conductivity. To obtain the porosity and pore size of the aerogels, mercury porosimetry measurements were then performed by an AutoPore IV 9500 porosimeter (Micromeritics, USA). The pyrolysis curves in N₂ from room temperature to 700 °C were obtained using a thermo-gravimetric analyzer (TGA, TGA/SDTA851e, Mettler-Toledo, Switzerland) under a heating rate of 20 °C·min⁻¹. The thermal conductivity of the resultant MPI aerogels at room temperature was measured by a Sweden Hotdisk TPS 2500S, using the transient plane source (TPS) method of ISO 22007-2 as the test standard. Besides, a WDW-1M electronic universal testing machine was used to evaluate their compressive strength. The crosshead speed and pretension for compression tests were set as 3 mm·min⁻¹ and 0.01 N, respectively.

Table 1. Summary of the parameters and properties of the prepared MPI aerogels

MPI aerogels	Density/g·cm⁻³	Shrinkage after preparation/%	Thermal conductivity /W·m⁻¹·k⁻¹	Young's modulus /MPa	Onset temperature (<i>T</i>_{-5wt%}) to decompose/°C
MPI-C-0	0.089	21.00	0.029	2.28	311.2
MPI-C-30	0.091	21.32	0.036	1.62	461.0
MPI-C-40	0.090	22.37	0.035	1.13	426.8
MPI-C-50	0.088	19.87	0.029	1.67	351.2
MPI-C-60	0.084	15.92	0.026	1.94	351.7
MPI-C-70	0.087	27.60	0.028	1.12	443.3
MPI-C-100	0.100	28.89	0.038	1.84	318.3
MPI-E-0	0.799	92.29	—	—	565.4
MPI-E-30	0.336	80.47	—	—	—
MPI-E-40	0.188	55.27	0.046	4.60	514.9
MPI-E-50	0.114	34.90	0.044	2.95	—
MPI-E-60	0.104	25.98	0.042	4.22	508.5
MPI-E-70	0.098	24.32	0.040	4.58	—
MPI-E-100	0.094	16.14	0.034	3.21	496.0

“—” in the table: Not measured.

3. Results and discussion

3.1 Morphology and structure

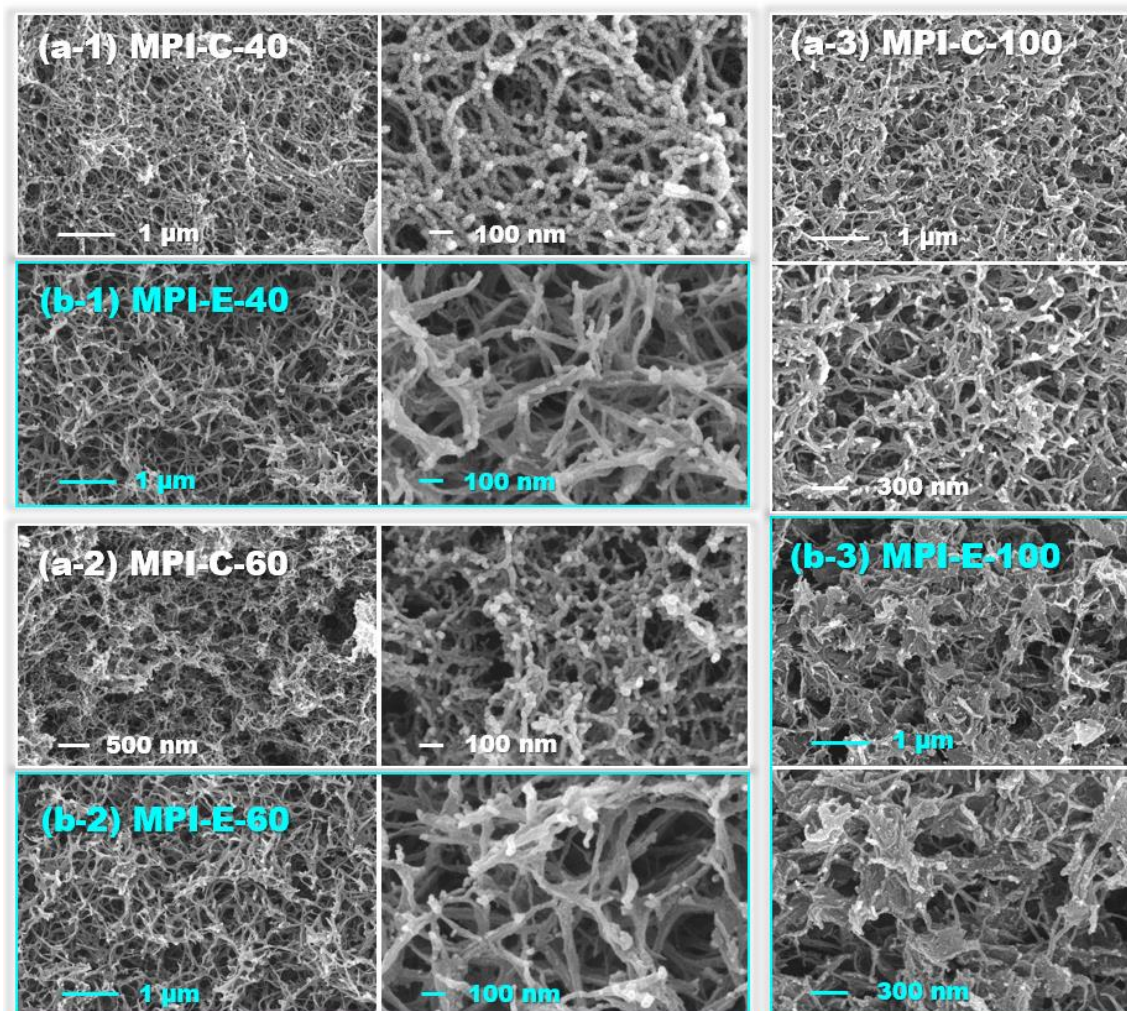


Figure 2. SEM images of three representative MPI-E aerogels, compared with those of the corresponding MPI-C ones.

The overall appearance of the prepared MPI aerogels is shown in the middle bottom of **Figure 1**. Similar to the previously reported MPI-C aerogels, the resultant MPI-E ones also have an almost regular cylindrical shape, indicating that supercritical ethanol drying did not deform the wet gels. However, the volume of the obtained MPI-E aerogels varies greatly with different DMBZ contents. The lower the content of DMBZ, the higher the shrinkage of MPI-E aerogel. As shown in **Table 1**, the volume shrinkage

of MPI-E-0 without DMBZ can reach up to 92.29 %, resulting in a quite large bulk density of $0.799 \text{ g}\cdot\text{cm}^{-3}$. This density value is far beyond the desired range of ultralight aerogels. With the incorporation of DMBZ, however, the size stability of the aerogel was greatly enhanced. The formed MPI-E aerogels tended to shrink less at higher DMBZ contents. The volume shrinkage of MPI-E-70 and MPI-E-100 was measured to be only 24.32 % and 16.14 %, respectively. The change of aerogel shrinkage with the increasing DMBZ content above is consistent with the observations of M. A. B. Meador [17]. The rigid structure of DMBZ-derived polyimides together with the less interaction among methyl-rich polymer chains should be responsible to the less shrinkage of MPI aerogels with more DMBZ incorporated.

The SEM images of three representative MPI-E aerogels and those of the corresponding MPI-C aerogels are depicted in **Figure 2**. It is apparent that the resultant MPI-E aerogels are also porous, but quite different from the MPI-C ones in term of pore size and morphology. As shown in **Figure 2 (b-1, b-2)**, the nanofibers that assembled into MPI-E-40 and MPI-E-60 are no longer as regular as those in MPI-C-40 and MPI-C-60. There appears severe fiber accumulation. The MPI-C-40 and MPI-C-60 appear as "stacked weeds", while the MPI-E-40 and MPI-E-60 with stronger fibrous branches present to be "clumped shrubs". These two MPI-E aerogels were assumed to be more robust than the MPI-C ones from CO_2 supercritical drying. This should be due to the harsher condition of supercritical ethanol drying ($276 \text{ }^\circ\text{C}$ and 8 MPa) for preparing MPI-E aerogels. By contrast, the temperature and pressure for supercritical CO_2 drying were only $45 \text{ }^\circ\text{C}$ and 7 MPa , respectively, much gentler than those of supercritical ethanol drying. The higher temperature of $276 \text{ }^\circ\text{C}$ causes MPI nanofibers to age more adequately, while the higher pressure of 8 MPa enables these nanofibers to adhere more closely, forming aerogels with a shrub-like branching microstructure. Also because of this, the

nanofiber-based aerogel pores tend to be larger. The distribution of these pores obtained by a mercury porosimeter can be seen in **Figure 3 (a)**. It is obvious that most of the pores in MPI-E aerogels are nano-sized, ranging from several to tens of nanometers. These nano-sized pores are conducive to guarantee MPI-E aerogels excellent thermal insulation performance, by depressing gas-phase heat transfer and elongating solid-phase conductive path. The results in **Figure 3 (b)** also indicate that the average pore diameter of these MPI-E aerogels increases with increasing DMBZ content. Meanwhile, the aerogel's porosity also shows a growing tendency with the increase of DMBZ content. The difference in volume shrinkage of MPI-E aerogels should be the main reason for this. The data in **Table 1** show that MPI-E aerogels with lower DMBZ contents suffer more severe shrinkage, resulting in denser bulk densities. That is, the less DMBZ in MPI-E aerogel, the higher solid content per unit volume of the aerogel, the lower porosity in other words. This explains why the porosity of MPI-E aerogels increases with the increase of DMBZ content. As to the pores in the aerogel, they also shrink as the aerogel shrinks. A greater shrinkage value therefore corresponds to smaller pore size, presented as smaller average pore diameter at lower DMBZ content.

The aggregation of nanofibers in MPI-C and MPI-E aerogels both becomes more serious with increasing DMBZ content. As shown in **Figure 2**, the morphology of MPI-E-100 without ODA contains a large deal of polymer flakes, somewhat similar to those of graphene and chitosan aerogels [22-24]. These polymer flakes are connected by dendritic short fibers to form a three-dimensional porous structure that is apparently different from the structure of MPI-E-40 and MPI-E-60. The formation of these flakes should be due to the larger scale phase separation at higher DMBZ content.

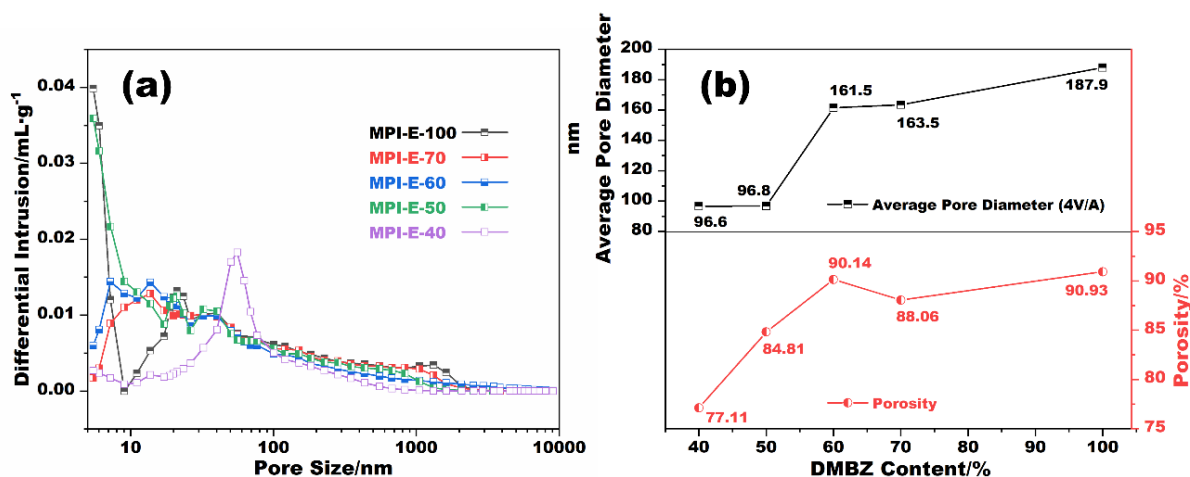


Figure 3. The variations of differential intrusion with pore size (a), which reflects the distribution of aerogel pores; The changes of average pore diameter and porosity of MPI-E aerogels with DMBZ content (b).

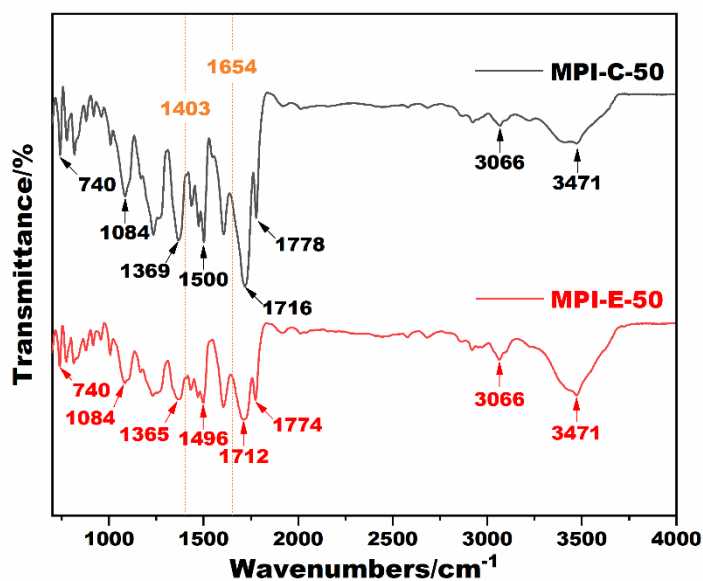


Figure 4. The FTIR spectra of the MPI-C-50 and MPI-E-50 aerogels.

The FTIR spectra of the obtained MPI-E-50 and MPI-C-50 aerogels are shown in **Figure 4**. From the plot of MPI-E-50, the characteristic peak centered around 3471 cm⁻¹ is mostly attributed to the stretching vibration of N-H [25]. These peaks at about 740 cm⁻¹, 1712 cm⁻¹ and 1774 cm⁻¹ are contributed to the bending, symmetric and asymmetric stretching vibrations of imide C=O, respectively [26-28]. The corresponding peaks for the stretching vibrations of C-N and C=C are located at 1365

cm^{-1} and 1496 cm^{-1} . From the whole sight, the FTIR spectrum of MPI-E-50 is almost the same as that of MPI-C-50. It can be given that supercritical ethanol drying has not changed the chemical structure of the aerogel. The result ensures that MPI-E aerogels will inherit the excellent comprehensive performance that MPI-C has. Note that, for both MPI-E-50 and MPI-C-50, no peaks were observed at the wavenumbers of 1403 cm^{-1} and 1654 cm^{-1} , which correspond to the C-N stretching vibrations and unreacted anhydride C=O present in PAA (polyamic acid, the precursor of PI) [29]. This indicates that the resultant MPI-E aerogels are also completely imidized like MPI-C.

3.2 Thermal properties

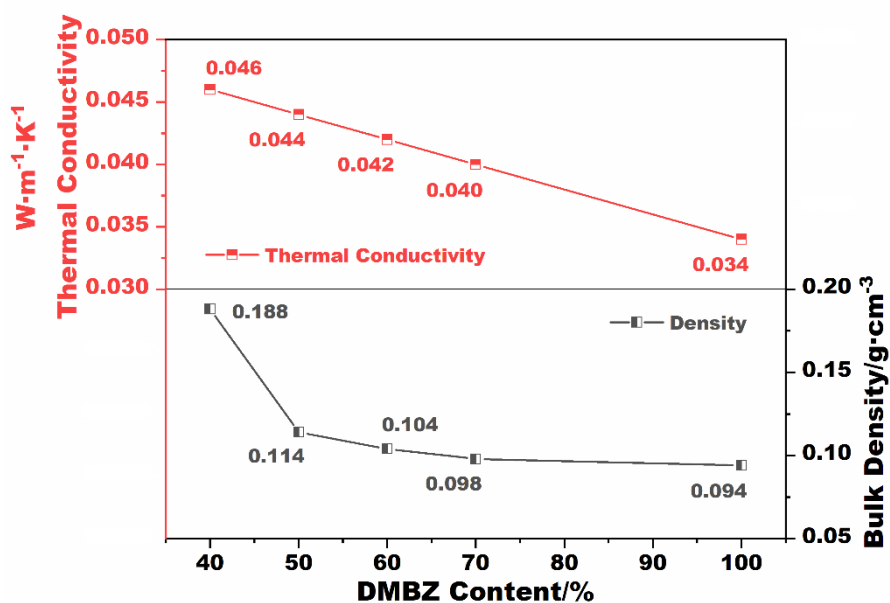


Figure 5. The variations of the thermal conductivity and bulk density of MPI-E aerogel with DMBZ content.

For MPI aerogels, the gas-phase and solid-phase conduction play a dominate role in heat transfer. Of the two, the solid-phase conductivity of an aerogel was reported to increase with increasing bulk density, while the gas-phase thermal conductivity increases with the increase of pore size and porosity [30, 31]. As shown in **Figure 5**, the

bulk density of the MPI-E aerogel decreases gradually from $0.188 \text{ g}\cdot\text{cm}^{-3}$ to $0.094 \text{ g}\cdot\text{cm}^{-3}$ with the increase of DMBZ content from 40 % to 100 %. The heat transfer due to solid-phase conduction therefore decreases as DMBZ content increases. In this regard, the MPI aerogel with a lower DMBZ content should have a higher thermal conductivity value. This is consistent with the test results. As the red curve in **Figure 5** shows, the aerogel's thermal conductivity represents an almost linear change with the increase of DMBZ content. The value decreases from $0.046 \text{ W}\cdot\text{m}^{-1}\cdot\text{k}^{-1}$ to $0.034 \text{ W}\cdot\text{m}^{-1}\cdot\text{k}^{-1}$ as DMBZ content increases from 40 % to 100 %. Note that, due to the large shrinkage of the MPI-E-0 and MPI-E-30 aerogels, adequate surfaces were not available for these two aerogels to conduct the thermal conductivity tests. Their behavior in thermal insulation therefore were not covered in this study. In addition to the solid-phase conduction, gas-phase heat conduction is another important aspect that cannot be ignored. The results by a mercury porosimeter have shown that the higher the content of DMBZ, the larger the average pore size and the higher the aerogel porosity (see **Figure 3**). That is to say, the gas-phase thermal conductivity of MPI-E aerogels increases with increasing DMBZ content. However, the thermal conductivity of MPI-E aerogel shows an opposite trend, revealing that the heat transfer inside MPI-E mainly depends on its solid skeletons. MPI-E aerogels with the lowest possible shrinkage and therefore loosest possible structure thus are more attractive for thermal insulation. On the contrary, if the MPI aerogel suffers severe volume shrinkage during use, its thermal insulation advantage will be greatly weakened due to the sharp rise in solid-phase conduction. This may further cause unwanted damage to the objects protected. Given these, MPI-E aerogels with high use stability that can avoid shrinking during use are exactly what we want.

From an overall perspective, the resultant MPI-E aerogels still perform quite well in thermal insulation, although their thermal conductivity is slightly larger than that of the

corresponding MPI-C aerogels. There is a reasonable prospect that MPI-E aerogels that combine the advantages of ultralow density ($0.094\text{-}0.188\text{ g}\cdot\text{cm}^{-3}$) and low thermal conductivity ($\sim 0.04\text{ W}\cdot\text{m}^{-1}\cdot\text{k}^{-1}$ at room temperature) are promising for thermal insulation applications.

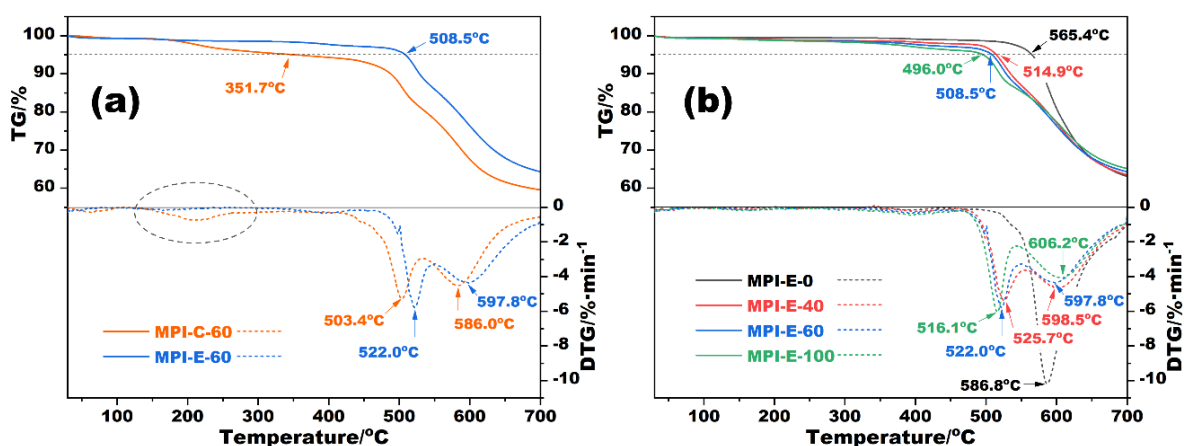


Figure 6. TG and DTG curves of MPI-C-60 and MPI-E-60 aerogels (a), as well as those of MPI-E aerogels with different DMBZ contents (b).

Figure 6 (a) compares the TD and DTG curves of the MPI-C-60 and MPI-E-60 aerogels. It is obvious that the MPI-C-60 aerogel suffers a significant weight loss within 150-300 °C, which should be the main reason for the severe shrinkage of MPI-C aerogels in use. Given that these aerogels were fully imidized, the removal of possible residual solvent (NMP with a normal boiling point of 202 °C), moisture and CO₂ adsorbed should be responsible. If supercritical drying was carried out with ethanol rather than CO₂, a much higher treatment temperature of 276 °C could remove the above residues more easily. Meanwhile, the aerogels had no chance to absorb CO₂ in the process of drying. The corresponding weight loss stage within 150-300 °C therefore disappeared, as the blue TG curve in **Figure 6 (a)** shows. This is the main difference between MPI-E and MPI-C aerogels in thermal decomposition. The TG curves of MPI-C-60 and MPI-E-60 in **Figure 6 (a)** then show a high degree of consistency as the temperature rises above 300 °C. The onset temperature ($T_{-5\text{wt}\%}$) for MPI-E-60 to decompose increases to 508.5 °C, indicative of greatly enhanced performance in thermal endurance. From the derivative

thermogravimetric (DTG) curves in the same figure, two weight loss peaks are seen for both MPI-C-60 and MPI-E-60 above 300 °C. The temperature of each peak (denoted as T_{p1} and T_{p2}) also increases after drying by supercritical ethanol, which further proves that the power of MPI aerogels against high temperatures were obviously enhanced by replacing CO₂ with ethanol for supercritical drying. Besides, the residue remained at 700 °C for MPI-E-60 is about 64.32 % of its initial mass, 4.75 % higher than that of MPI-C-60, indicating that MPI-E-60 has better ability to form char.

Figure 6 (b) gives the TD and DTG curves of MPI-E aerogels with different DMBZ contents. The results in this figure and **Table 2** reveal that the aerogel's onset temperature to decompose decreases gradually with the increase of DMBZ content. As shown, the MPI-E-0 aerogel without DMBZ has the highest $T_{-5wt\%}$ value of 565.4 °C while MPI-E-100 has the lowest $T_{-5wt\%}$ value of 496.0 °C. This is because the polyimide chains derived from ODA decompose at a higher temperature than the DMBZ-derived ones, in accordance with several other reports [32-34]. The presence of pendent methyl groups should be responsible for the relatively lower decomposition temperature of the DMBZ containing aerogels. Even so, most of the MPI-E aerogels almost didn't decompose before 500 °C, desirable by high temperature applications. As to the pyrolysis residue at 700 °C given in **Table 2**, it slightly increases with increasing DMBZ content. The residue remained at 700 °C for MPI-E-100 was measured to be 65.14 %, just about 2 % higher than that of MPI-E-0. It can be concluded that increasing the content of DMBZ in MPI-E can not only effectively improve the aerogel's thermal insulation by reducing its shrinkage during preparation, but increase its carbon residue after pyrolysis. This is attractive for high-temperature thermal insulation applications, but comes at the cost of a slight decrease in thermal endurance.

Table 2. Characteristic parameters and residue at 700 °C of MPI-E aerogels with different DMBZ contents as well as MPI-C-60.

Sample	$T_{-5wt\%}/^{\circ}\text{C}$	$T_{p1}/^{\circ}\text{C}$	$T_{p2}/^{\circ}\text{C}$	Residue at 700 °C/%
MPI-E-0	565.4	-	586.8	63.11
MPI-E-40	514.9	525.7	598.5	63.52
MPI-C-60	351.7	503.4	586.0	59.57

MPI-E-60	508.5	522.0	597.8	64.32
MPI-E-100	496.0	516.1	606.2	65.14

3.3 Mechanical Strength

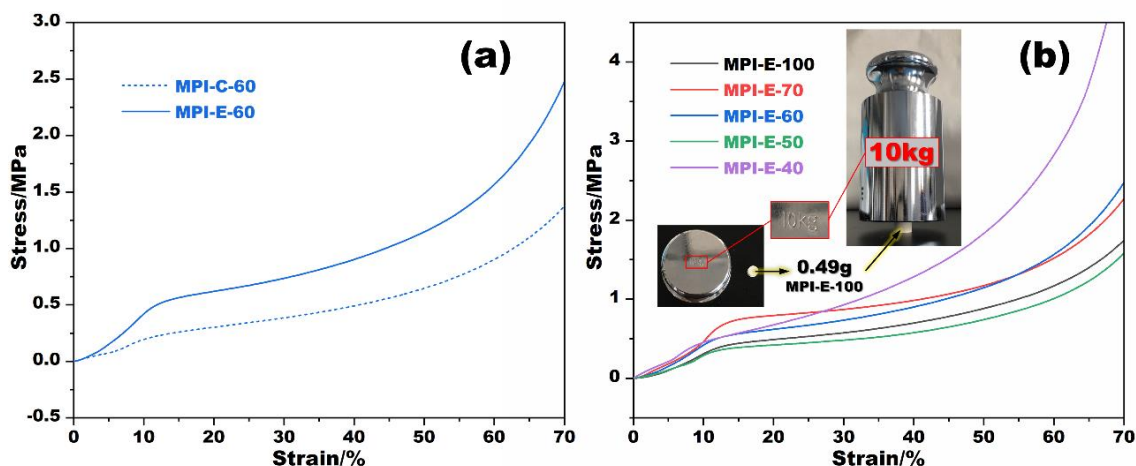


Figure 7. Compressive stress-strain curves of MPI-C-60 and MPI-E-60 (a), as well as those of MPI-E aerogels with different DMBZ contents (b).

The compressive stress-strain curves of MPI-E aerogels with a maximum strain of 70 % are presented in **Figure 7**. It is clear from **Figure 7 (a)** that the MPI-E-60 aerogel bears greater stress than MPI-C-60 at the same strain. The Young's modulus of MPI-E-60 was calculated to be 4.22 MPa, more than twice that of the MPI-C-60 (see **Table 1**). This can be understood from two aspects: the first one is that the MPI-E-60 aerogel with a bulk density of $0.104 \text{ g}\cdot\text{cm}^{-3}$ is denser than MPI-C-60 ($0.084 \text{ g}\cdot\text{cm}^{-3}$). That is, there are more polymer branches per unit cross section against external forces for MPI-E-60, shown as higher compressive strength. The second reason is that the fibrous skeletons of MPI-E-60 are much stronger than those of MPI-C-60, as the SEM images in **Figure 2** show. These are the reasons why MPI-E-60 is superior to MPI-C-60 in compression resistance.

Figure 7 (b) shows the stress-strain curves of MPI-E aerogels with different DMBZ contents. The results indicate that all MPI-E aerogels undergo three stages

during the compression. The first one at about strain < 10 % is known as the elastic region, in which stress increases almost linearly with the strain. After that, the energy absorbed during compression dissipates due to pore collapse, resulting in a relatively slow increase in stress. This is often referred to as the plateau region. If the strain further increases to more than 60 %, a densification region then occurs. Unfortunately, no significant correlation between the mechanical strength of MPI-E aerogels and DMBZ content was found. This is mainly because the mechanical performance of an aerogel depends not only on its density but also its structure. For the MPI-E-40 with a severe shrinkage of 55.27 vol.%, its dense structure contributes to its higher compressive strength. But for the others with less shrinkage and therefore lower densities, their resistant to external forces drops. Even so, the Young's modulus of the aerogel with a DMBZ content varying from 40 % to 100 % is still as high as 2.95-4.60 MPa, indicative of considerable compressive strength. As shown in **Figure 7 (b)**, a 0.49 g MPI-E-100 can easily support a 10 kg counterpoise, more than 20,000 times its own weight. This is a living proof of the excellent mechanical strength of MPI-E aerogels prepared from supercritical ethanol drying.

3.4 Shape Stability

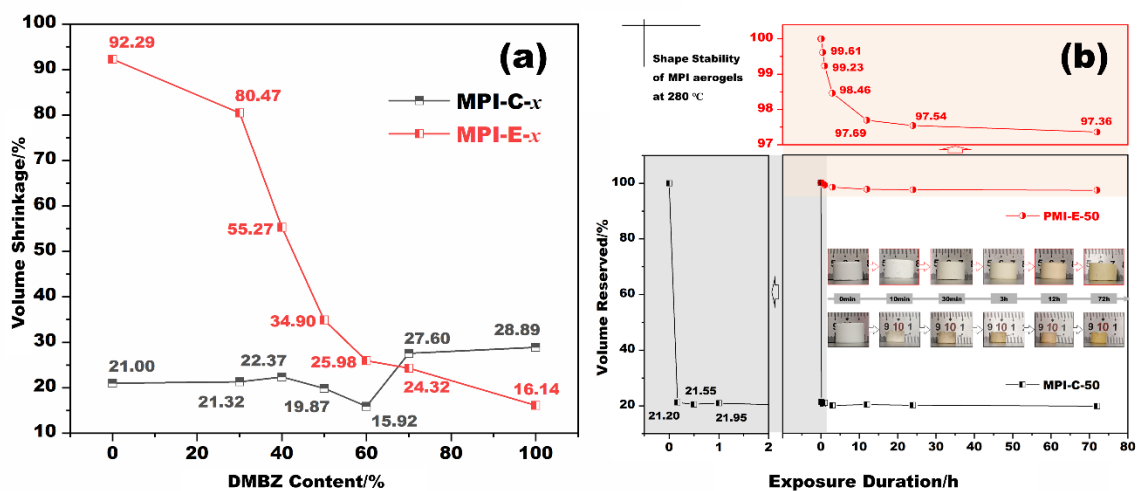


Figure 8. The shrinkage of MPI-E and MPI-C aerogels occurred in the process of preparation (a); the volume shrinkage and appearance changes of MPI-E-50 and MPI-C-50 after treated at 280 °C for different periods of duration (b).

Figure 8 (a) plots the shrinkage of the resultant MPI-E aerogels with different DMBZ contents in the process of preparation. As we discussed above, the lower the content of DMBZ, the higher the shrinkage of MPI-E aerogel. Besides, due to the harsh condition of supercritical ethanol drying, most of the MPI-E aerogels suffer a more severe shrinkage than the MPI-C ones during preparation. The shrinkage of MPI-E-70 and MPI-E-100, however, is lower than that of the corresponding MPI-C ones. Take MPI-E-100 as an example, it shrank by only 16.14 % of its initial volume, lower than the 28.89 % of MPI-C-100. In other words, MPI-E-100 has a better preparation shape stability than MPI-C-100. This is mainly due to the rigid nature of DMBZ and the more robust structure of MPI-E aerogels. Therefore, supercritical ethanol drying can produce MIP aerogels that experience much lower volume shrinkage in the process of preparation, but this requires strict control of DMBZ content in hybrid diamines. From the present study, to obtain MPI-E aerogels that shrink less than those prepared from supercritical CO₂ drying, the DMBZ content should be higher than 70 %.

To explore the shape stability of MPI-E aerogels for high-temperature applications, thermal treatments were then performed at 280 °C. The volume changes of MPI-C-50 and MPI-E-50 with exposure time can be seen in **Figure 8 (b)**. It is observed that the MPI-C-50 shrank to about only 20 % of its original volume after just 10 min of heat treatment at 280 °C. This brings great unreliability to the use of MPI-C aerogels. As to the MPI-E-50, it shrank by less than 3%. The volume of MPI-E-50 remained almost unchanged at about 97.5 % after 24 h. As mentioned at the very beginning, the purpose of drying MPI aerogels with supercritical ethanol is to allow the aerogels to endure the

high temperature of supercritical ethanol in advance, and thereby to avoid possible shrinkage when they are used at such high temperatures. The results here are consistent with what we intended in the first place. It has been proved that the resultant MPI-E aerogels does have the desired advantage of shape stability in use. In addition, the color of both MPI-E-50 and MPI-C-50 also varied from white to yellow with increasing exposure time. The MPI-C-50 also shows a darker apparent color due to its more severe volume shrinkage. This was caused by the thermal aging of polyimide, and will not degrade the aerogel's shape stability in use.

4. Conclusions

In this study, a series of melamine-crosslinked polyimide (MPI) aerogels were prepared from supercritical ethanol drying, to avoid possible severe shrinkage suffered in use. Compared with the MPI-C ones, the resultant MPI-E aerogels possess a more robust branching structure, which brings them enhanced mechanical strength. The MPI-E-100 aerogel can easily support a counterpoise more than 20, 000 times its own weight. Besides, MPI-E aerogels are also good at thermal insulation with thermal conductivity values varying from $0.034 \text{ W}\cdot\text{m}^{-1}\cdot\text{k}^{-1}$ to $0.046 \text{ W}\cdot\text{m}^{-1}\cdot\text{k}^{-1}$. More importantly, the resultant MPI-E aerogels that endured the baptism of supercritical ethanol drying in advance almost no longer lose weight before $300 \text{ }^\circ\text{C}$. As a result, the severe in-use shrinkage of MPI aerogels at high temperatures is well solved, expressed as greatly improved shape stability. In addition, changing the drying condition for preparing MPI aerogels to supercritical ethanol drying did not change the aerogel's chemical structure. The MPI-E aerogels therefore are still excellent in thermal endurance and char forming. Their onset temperature to decompose is around $500 \text{ }^\circ\text{C}$ and the residue at $700 \text{ }^\circ\text{C}$ is more than 63 % of their initial weight. Given these, MPI-E aerogels with powerful mechanical strength, excellent thermal insulation and greatly improved shape stability will be promising for

diverse applications.

Acknowledgements

This work was supported by National Natural Science Foundation of China (Grant No. 51904312), Shandong “Taishan Youth Scholar Program (No. tsqn201909100)” and Civil Aviation University of China (2020KYQD115).

Compliance with ethical standards

Conflict of interest: The authors declare that they have no conflict of interest.

References

- [1] T. Wang, M. Long, H. Zhao, B. Liu, H. Shi, W. An, S. Li, S. Xu, Y. Wang, An ultralow-temperature superelastic polymer aerogel with high strength as a great thermal insulator under extreme conditions, *J. Mater. Chem. A* 8 (2020) 18698-18706. <https://doi.org/10.1039/D0TA05542E>.
- [2] H. Maleki, N. Hüsing, Current status, opportunities and challenges in catalytic and photocatalytic applications of aerogels: Environmental protection aspects, *Appl. Catal. B-Environ.* 221 (2018) 530-555. <https://doi.org/10.1016/j.apcatb.2017.08.012>.
- [3] B.F. Martins, P.V.O. de Toledo, D.F.S. Petri, Hydroxypropyl methylcellulose based aerogels: Synthesis, characterization and application as adsorbents for wastewater pollutants, *Carbohydr. Polym.* 155 (2017) 173-181. <https://doi.org/10.1016/j.carbpol.2016.08.082>.
- [4] Z. Qian, Z. Wang, N. Zhao, J. Xu, Aerogels derived from polymer nanofibers and their applications, *Macromol. Rapid Comm.* 39 (2018) 1700724. <https://doi.org/10.1002/marc.201700724>.
- [5] K. Wu, W. Dong, Y. Pan, J. Cao, Y. Zhang, D. Long, Lightweight and flexible phenolic aerogels with three-dimensional foam reinforcement for acoustic and thermal insulation, *Ind. Eng. Chem. Res.* 60 (2021) 1241-1249. <https://doi.org/10.1021/acs.iecr.0c05010>.
- [6] Y. Xiao, L. Li, F. Liu, S. Zhang, J. Feng, Y. Jiang, J. Feng, Compressible, flame-resistant and thermally insulating fiber-reinforced polybenzoxazine aerogel composites, *Materials* 13 (2020) 2809. <https://doi.org/10.3390/ma13122809>.
- [7] P. Paraskevopoulou, D. Chriti, G. Raptopoulos, G.C. Anyfantis, Synthetic polymer aerogels in particulate form, *Materials* 12 (2019) 1543. <https://doi.org/10.3390/ma12091543>.
- [8] A. Shinko, S.C. Jana, M.A.B. Meador, Crosslinked polyurea aerogels with controlled porosity, *RSC Adv.* 5 (2015) 105329-105338. <https://doi.org/10.1039/C5RA20788F>.
- [9] Z. Liu, J. Lyu, D. Fang, X. Zhang, Nanofibrous Kevlar aerogel threads for thermal insulation in harsh environments, *ACS Nano* 13 (2019) 5703-5711. <https://doi.org/10.1021/acsnano.9b01094>.
- [10] X. Zhang, N. Li, Z. Hu, J. Yu, Y. Wang, J. Zhu, Direct fabrication of poly(p-phenylene terephthalamide) aerogel and its composites with great thermal insulation and infrared stealth, *Chem. Eng. J.* 388 (2020) 124310. <https://doi.org/10.1016/j.cej.2020.124310>.
- [11] T. Wu, J. Dong, K. De France, M. Li, X. Zhao, Q. Zhang, Fabrication of polyimide aerogels cross-

- linked by a cost-effective amine-functionalized hyperbranched polysiloxane (NH₂-HBPSi), ACS Appl. Polym. Mater. 2 (2020) 3876-3885. <https://doi.org/10.1021/acsapm.0c00563>.
- [12] X. Li, G. Dong, Z. Liu, X. Zhang, Polyimide aerogel fibers with superior flame resistance, strength, hydrophobicity, and flexibility made via a universal Sol-Gel confined transition strategy, ACS Nano 15 (2021) 4759-4768. <https://doi.org/10.1021/acsnano.0c09391>.
- [13] S. Qiao, S. Kang, J. Zhu, Y. Wang, J. Yu, Z. Hu, Facile strategy to prepare polyimide nanofiber assembled aerogel for effective airborne particles filtration, J. Hazard. Mater. 415 (2021) 125739. <https://doi.org/10.1016/j.jhazmat.2021.125739>.
- [14] N. Diascorn, S. Calas, H. Sallée, P. Achard, A. Rigacci, Polyurethane aerogels synthesis for thermal insulation-textural, thermal and mechanical properties, J. Supercrit. Fluid. 106 (2015) 76-84. <https://doi.org/10.1016/j.supflu.2015.05.012>.
- [15] J.P. Randall, M.A.B. Meador, S.C. Jana, Tailoring mechanical properties of aerogels for aerospace applications, ACS Appl. Mater. Inter. 3 (2011) 613-626. <https://doi.org/10.1021/am200007n>.
- [16] S. Liu, W. Chen, X. Zhou, Polyimide aerogels using melamine as an economical yet effective crosslinker, J. Porous Mat. 28 (2021) 1155-1165. <https://doi.org/10.1007/s10934-021-01066-4>.
- [17] M.A.B. Meador, C.R. Alemán, K. Hanson, N. Ramirez, S.L. Vivod, N. Wilmoth, L. McCorkle, Polyimide aerogels with amide cross-links: A low cost alternative for mechanically strong polymer aerogels, ACS Appl. Mater. Inter. 7 (2015) 1240-1249. <https://doi.org/10.1021/am507268c>.
- [18] Z. Zhu, H. Yao, F. Wang, J. Dong, K. Wu, J. Cao, D. Long, Fiber reinforced polyimide aerogel composites with high mechanical strength for high temperature insulation, Macromol. Mater. Eng. 304 (2019) 1800676. <https://doi.org/10.1002/mame.201800676>.
- [19] Y. Shen, D. Li, B. Deng, Q. Liu, H. Liu, T. Wu, Robust polyimide nano/microfibre aerogels welded by solvent-vapour for environmental applications, Roy. Soc. Open Sci. 6 (2019) 190596. <https://doi.org/10.1098/rsos.190596>.
- [20] X. Zhang, X. Zhao, T. Xue, F. Yang, W. Fan, T. Liu, Bidirectional anisotropic polyimide/bacterial cellulose aerogels by freeze-drying for super-thermal insulation, Chem. Eng. J. 385 (2020) 123963. <https://doi.org/10.1016/j.cej.2019.123963>.
- [21] G. Xu, M. Li, T. Wu, C. Teng, Highly compressible and anisotropic polyimide aerogels containing aramid nanofibers, React. Funct. Polym. 154 (2020) 104672. <https://doi.org/10.1016/j.reactfunctpolym.2020.104672>.
- [22] C. Yue, J. Feng, J. Feng, Y. Jiang, Low-thermal-conductivity nitrogen-doped graphene aerogels for thermal insulation, RSC Adv. 6 (2016) 9396-9401. <https://doi.org/10.1039/C5RA23236H>.
- [23] W.S. Kim, S.Y. Moon, J. Koyanagi, T. Ogasawara, Three-dimensional porous graphene-based ultra-lightweight aerofoam exhibiting good thermal insulation, Adv. Compos. Mater. 25 (2016) 105-113. <https://doi.org/10.1080/09243046.2016.1193939>.
- [24] J. Mao, S. Li, C. He, Y. Tang, Z. Chen, J. Huang, Y. Lai, Robust amphiprotic konjac glucomannan cross-linked chitosan aerogels for efficient water remediation, Cellulose 26 (2019) 6785-6796. <https://doi.org/10.1007/s10570-019-02549-z>.
- [25] S. Xi, X. Wang, T. Liu, Z. Zhang, X. Zhang, J. Shen, Moisture-resistant and mechanically strong polyimide-polymethylsilsesquioxane hybrid aerogels with tunable microstructure, Macromol. Mater. Eng. 306 (2021) 2000612. <https://doi.org/10.1002/mame.202000612>.
- [26] X. Zhang, W. Li, P. Song, B. You, G. Sun, Double-cross-linking strategy for preparing flexible, robust, and multifunctional polyimide aerogel, Chem. Eng. J. 381 (2020) 122784. <https://doi.org/10.1016/j.cej.2019.122784>.

- [27] Z. Zhang, Y. Pan, L. Gong, X. Yao, X. Cheng, Y. Deng, Mechanically strong polyimide aerogels cross-linked with low-cost polymers, *RSC Adv.* 11 (2021) 10827-10835. <https://doi.org/10.1039/D0RA10633J>.
- [28] Y. Shen, D. Li, L. Wang, Y. Zhou, F. Liu, H. Wu, B. Deng, Q. Liu, Superelastic polyimide nanofiber-based aerogels modified with silicone nanofilaments for ultrafast oil/water separation, *ACS Appl. Mater. Inter.* 13 (2021) 20489-20500. <https://doi.org/10.1021/acsami.1c01136>.
- [29] X. Hou, R. Zhang, D. Fang, Flexible, fatigue resistant, and heat-insulated nanofiber-assembled polyimide aerogels with multifunctionality, *Polym. Test.* 81 (2020) 106246. <https://doi.org/10.1016/j.polymertesting.2019.106246>.
- [30] B. Li, S. Jiang, S. Yu, Y. Chen, X. Tang, X. Wu, Y. Zhong, X. Shen, S. Cui, Co-polyimide aerogel using aromatic monomers and aliphatic monomers as mixing diamines, *J. Sol-Gel Sci. Techn.* 88 (2018) 386-394. <https://doi.org/10.1007/s10971-018-4800-1>.
- [31] Y. Wu, W. Zhang, R. Yang, Ultralight and low thermal conductivity polyimide-polyhedral oligomeric silsesquioxanes aerogels, *Macromol. Mater. Eng.* 303 (2018) 1700403. <https://doi.org/10.1002/mame.201700403>.
- [32] M.A.B. Meador, E.J. Malow, R. Silva, S. Wright, D. Quade, S.L. Vivod, H. Guo, J. Guo, M. Cakmak, Mechanically strong, flexible polyimide aerogels cross-linked with aromatic triamine, *ACS Appl. Mater. Inter.* 4 (2012) 536-544. <https://doi.org/10.1021/am2014635>.
- [33] H. Guo, M.A.B. Meador, L. S. McCorkle, D.A. Scheiman, J.D. McCrone, B. Wilkewitz, Poly(maleic anhydride) cross-linked polyimide aerogels: synthesis and properties, *RSC Adv.* 6 (2016) 26055-26065. <https://doi.org/10.1039/C6RA01013J>.
- [34] T. Wu, J. Dong, G. Xu, F. Gan, X. Zhao, Q. Zhang, Attapulgite-reinforced polyimide hybrid aerogels with high dimensional stability and excellent thermal insulation property, *Polymer* 176 (2019) 196-205. <https://doi.org/10.1016/j.polymer.2019.05.007>.